Astronomy & Astrophysics

Observations of Sagittarius A* during the pericenter passage of the G2 object with MAGIC

M. L. Ahnen[1], S. Ansoldi[2], L. A. Antonelli[3], P. Antoranz[4], C. Arcaro[5], A. Babic[6], B. Banerjee[7], P. Bangale[8],
U. Barres de Almeida[8,24], J. A. Barrio[9], J. Becerra González[10,34], W. Bednarek[11], E. Bernardini[12,26], A. Berti[2,27],
B. Biasuzzi[2], A. Biland[1], O. Blanch[13], S. Bonnefoy[9], G. Bonnoli[4], F. Borracci[8], T. Bretz[14,28], S. Buson[5,25,35],
A. Carosi[3], A. Chatterjee[7], R. Clavero[10,34], P. Colin[8], E. Colombo[10,34], J. L. Contreras[9], J. Cortina[13], S. Covino[3],
P. Da Vela[4], F. Dazzi[8], A. De Angelis[5], B. De Lotto[2], E. de Oña Wilhelmi[15], F. Di Pierro[3], M. Doert[16], A. Domínguez[9],
D. Dominis Prester[6], D. Dorner[14], M. Doro[5], S. Einecke[16], D. Eisenacher Glawion[14], D. Elsaesser[16],
M. Engelkemeier[16], V. Fallah Ramazani[17], A. Fernández-Barral[13], D. Fidalgo[9], M. V. Fonseca[9], L. Font[18],
K. Frantzen[16], C. Fruck[8,★], D. Galindo[19], R. J. García López[10,34], M. Garczarczyk[12], D. Garrido Terrats[18], M. Gaug[18],
P. Giammaria[3], N. Godinović[6], A. González Muñoz[13], D. Gora[12], D. Guberman[13], D. Hadasch[20], A. Hahn[8],
M. Hayashida[20], J. Herrera[10,34], J. Hose[8], D. Hrupec[6], G. Hughes[1], W. Idec[11], K. Kodani[20], Y. Konno[20], H. Kubo[20],
J. Kushida[20], A. La Barbera[3], D. Lelas[6], E. Lindfors[17], S. Lombardi[3], F. Longo[2,27], M. López[9], R. López-Coto[13,29],
P. Majumdar[7], M. Makariev[21], K. Mallot[12], G. Maneva[21], M. Manganaro[10,34], K. Mannheim[14], L. Maraschi[3],
B. Marcote[19], M. Mariotti[5], M. Martínez[13], D. Mazin[8,30], U. Menzel[8], J. M. Miranda[4], R. Mirzoyan[8], A. Moralejo[13],
E. Moretti[8], D. Nakajima[20], V. Neustroev[17], A. Niedzwiecki[11], M. Nievas Rosillo[9], K. Nilsson[17,31], K. Nishijima[20],
K. Noda[8], L. Nogués[13], A. Overkemping[16], S. Paiano[5], J. Palacio[13], M. Palatiello[2], D. Paneque[8], R. Paoletti[4],
J. M. Paredes[19], X. Paredes-Fortuny[19], G. Pedaletti[12], M. Peresano[2], L. Perri[3], M. Persic[2,32], J. Poutanen[17],
P. G. Prada Moroni[22], E. Prandini[1,33], I. Puljak[6], J. R. Garcia[8], I. Reichardt[5], W. Rhode[16], M. Ribó[19], J. Rico[13],
T. Saito[20], K. Satalecka[12], S. Schroeder[16], T. Schweizer[8], S. N. Shore[22], A. Sillanpää[17], J. Sitarek[11], I. Snidaric[6],
D. Sobczynska[11], A. Stamerra[3], T. Steinbring[14], M. Strzys[8], T. Surić[6], L. Takalo[17], F. Tavecchio[3], P. Temnikov[21],
T. Terzić[6], D. Tescaro[5], M. Teshima[8,30], J. Thaele[16], D. F. Torres[23], T. Toyama[8], A. Treves[2], G. Vanzo[10,34],
V. Verguilov[21], I. Vovk[8,★], J. E. Ward[13,★], M. Will[10,34], M. H. Wu[15], and R. Zanin[19,29]

(Affiliations can be found after the references)

ABSTRACT

Context. We present the results of a multi-year monitoring campaign of the Galactic center (GC) with the MAGIC telescopes. These observations were primarily motivated by reports that a putative gas cloud (G2) would be passing in close proximity to the super-massive black hole (SMBH), associated with Sagittarius A*, located at the center of our galaxy. This event was expected to give astronomers a unique chance to study the effect of in-falling matter on the broad-band emission of a SMBH.
Aims. We search for potential flaring emission of very-high-energy (VHE; ≥100 GeV) gamma rays from the direction of the SMBH at the GC due to the passage of the G2 object. Using these data we also study the morphology of this complex region.
Methods. We observed the GC region with the MAGIC Imaging Atmospheric Cherenkov Telescopes during the period 2012–2015, collecting 67 h of good-quality data. In addition to a search for variability in the flux and spectral shape of the GC gamma-ray source, we use a point-source subtraction technique to remove the known gamma-ray emitters located around the GC in order to reveal the TeV morphology of the extended emission inside that region.
Results. No effect of the G2 object on the VHE gamma-ray emission from the GC was detected during the 4 yr observation campaign. We confirm previous measurements of the VHE spectrum of Sagittarius A*, and do not detect any significant variability of the emission from the source. Furthermore, the known VHE gamma-ray emitter at the location of the supernova remnant G0.9+0.1 was detected, as well as the recently discovered VHE source close to the GG radio arc.

Key words. Galaxy: center – gamma rays: general – black hole physics

1. Introduction

The Galactic center region. The central region of our galaxy is very densely populated with a large variety of astrophysical objects, many of which may be sites of extreme particle acceleration and hence gamma-ray emission (van Eldik 2015; Aharonian et al. 2006a,b). Multi-wavelength observations of this region and their interpretation have always been challenging due to a combination of source confusion and absorption along the line of sight (Genzel et al. 2010).

Regardless, the Galactic center (GC) region has been observed by several astronomical instruments over the previous three decades. The most precise data, especially regarding

---

★ Corresponding authors:
Christian Fruck, e-mail: fruck@mpp.mpg.de;
Ievgen Vovk, e-mail: ievgen.vovk@mpp.mpg.de;
and John Ennis Ward, e-mail: jward@ifae.es

angular resolution, are coming from observations in the near IR (4×10^{-2} arcsec resolution, Genzel et al. 2003) and radio (5×10^{-4} arcsec resolution, Bower et al. 2014) using large scale instruments like the Very Large Telescope (VLT, near IR), the Very Large Array (VLA, radio) and the Very Long Baseline Array (VLBA, radio). In the X-ray regime, the *Chandra* and *NuStar* satellites offer excellent angular (*Chandra*: 0.5 arcsec, *NuStar*: 9.5 arcsec) and energy resolution for the study of the GC region (Baganoff et al. 2000; Weisskopf et al. 2000; Mori et al. 2015; Kistler 2015).

These observations have revealed several astrophysical sources in the GC region. Among those, the compact radio source Sagittarius A* (Sgr A*) is of a particular interest, and is generally accepted to be associated with the $4 \times 10^6 \, M_\odot$ black hole at the center of our galaxy. The apparent size of the event horizon of the supermassive black hole (SMBH) is estimated to be about 10^{-5} arcsec (Fish et al. 2011).

In the X-ray domain, Sgr A* is an unexpectedly faint emitter ($L_x \approx 2 \times 10^{33}$ erg s^{-1} in the 2–10 keV band, Baganoff et al. 2003) that does however display sporadic X-ray flaring activity on timescales from minutes to hours (Baganoff et al. 2001). Ponti et al. (2015) presented an analysis of 15 yr of X-ray observations (from September 1999 until November 2014) of Sgr A* taken with the *XMM-Newton* and *Chandra* observatories. Interestingly, this study found an increase by a factor of 2–3 in the X-ray flare luminosity of Sgr A* between 2013 and 2014 (although with a significance of only 3.5σ), along with an increase in the rate of bright and very-bright X-ray flares with a significance of 3.3σ. It should be noted that the authors acknowledge that this increase in measured flaring activity may purely be a sampling issue due to an increase in the monitoring frequency of Sgr A* during that period.

The GC region has been also extensively observed in the high energy (HE; $\geq$100 MeV) gamma-ray regime with the EGRET (Mayer-Hasselwander et al. 1998) and *Fermi* (Porter et al. 2015) instruments, and in the very-high-energy (VHE; $\geq$100 GeV) regime with Imaging Atmospheric Cherenkov Telescopes (IACTs). The first strong hints for a detection of VHE gamma rays from the GC were reported by CANGAROO II (Enomoto et al. 2003), and one year later by the Whipple collaboration (Kosack et al. 2004). The H.E.S.S. collaboration in the same year reported a highly significant ($\sim$10σ) detection of a source at the GC with spectral index $\alpha = 2.2$, designated as HESS J1745-290 (Aharonian et al. 2004). MAGIC observations confirmed these results with a compatible flux and spectral index (Albert et al. 2006).

Recently, new observational results from H.E.S.S. and VERITAS have been published (H.E.S.S. Collaboration 2016; Archer et al. 2014, 2016; Aharonian et al. 2009). In particular, data from the continued H.E.S.S. observations of the region around the GC suggest that the Sgr A* black hole is able to accelerate particles to PeV energies (H.E.S.S. Collaboration 2016). Observations by VERITAS of the GC ridge have revealed the presence of a new source (VER J1746-289) near the GC radio arc (GCA; Archer et al. 2016). Previously, H.E.S.S., MAGIC and VERITAS have reported on a new source of VHE emission from the same region near the GC (Lemiere et al. 2015; Fruck et al. 2015; Smith 2015), which we will also address here.

The source and mechanism responsible for the production of HE and VHE gamma radiation from the GC still remain an active topic of discussion. Sgr A* and the pulsar wind nebula G 359.95-0.04 (Wang et al. 2006; Hinton & Aharonian 2007) are the leading candidates in the region since Aharonian et al. (2009) and Acero et al. (2010) claimed to be able to rule out the nearby supernova remnant Sagittarius A East as a main contributor to the TeV emission. Several models for the production of high-energy radiation from Sgr A* itself have been presented, including leptonic (Kusunose & Takahara 2012; Atoyan & Dermer 2004), hadronic (Fatuzzo & Melia 2012; Linden et al. 2012; Ballantyne et al. 2011; Chernyakova et al. 2011; Wang et al. 2009; Aharonian & Neronov 2005) and hybrid (Guo et al. 2013) scenarios.

The G2 object. Gillessen et al. (2012) reported the VLT infrared detection of a gas cloud with an estimated mass on the order of 3 Earth masses ($\sim$10^{-5} $M_\odot$) on a highly eccentric orbit towards the central SMBH of our galaxy. Extrapolating the orbit led to a predicted pericenter passage in mid-2013 at a distance of about 3100 Schwarzschild radii (R_g) from the SMBH. After continuous measurements these numbers were updated to September 2013 and 2200 R_g (Gillessen et al. 2013a). Gillessen et al. (2013b) reported that part of the gas cloud was observed past the pericenter approach by early 2013 and that the whole process would probably extend over at least one whole year. Other observations of the G2 object have resulted in the suggestion that G2 may in fact be the product of a binary-star merger (Witzel et al. 2014; Meyer et al. 2014) or a young star with $m \lesssim 3 \, M_\odot$ (Zajacek et al. 2015) as opposed to a gas cloud.

Predictions concerning the fate of the object and its possible influence on the accretion rate of the SMBH at the GC were highly dependent on the assumed density and structure of G2 as well as the physical environment close to Sgr A*. These predictions ranged from no observable effects to strong flaring activity of Sgr A* (Schartmann et al. 2012; Giannios & Sironi 2013). Bartos et al. (2013) suggested that G2 may also interact with stellar-mass black holes expected to exist in the vicinity of Sgr A*.

Despite all of the uncertainties concerning the nature of this object, order-of-magnitude estimations can be made in order to put limits on the potential effects of a SMBH accretion event on the observed gamma-ray flux of Sgr A*. The maximal amount of energy that can be released in the process of accretion of an object with mass m onto a black hole is between 6% and 42% of the object's rest-mass energy (mc^2), depending on the black hole angular momentum (Shapiro & Teukolsky 1983). Assuming that G2, with a mass of $\sim$10^{-5} $M_\odot$, is accreted onto Sgr A* over the duration of a year (i.e. 30 times higher than the baseline accretion rate estimated by Yusef-Zadeh et al. 2015) and estimating the total accretion-disk luminosity to be $\sim$10^{-1} $\dot{M}c^2$ (Eq. (14.5.3) from Shapiro & Teukolsky 1983), the power released would be of the order of $10^{40.5}$–$10^{41.5}$ erg s^{-1}. If only a small fraction of this power is used to accelerate high-energy particles, the resulting photon flux may well be comparable to the observed gamma-ray luminosity of the GC ($\sim$10^{35} erg s^{-1} above 0.5 TeV).

Even considering the uncertainties in the predicted emission across all wavelengths, the possibility of observing in-falling matter onto the central SMBH of the galaxy was regarded as an interesting scientific opportunity and triggered MAGIC monitoring of the GC over the period 2012–2015.

Despite the fact that recent observations in the near-infrared (Ghez et al. 2014) appear to show that the G2 object has passed by Sgr A* largely unaffected, and that observations reported by Bower et al. (2015) in the radio, millimeter and submillimeter wavebands taken during the apparent periastron passage of G2 show that the flux density and spectrum of Sgr A* has remained stable (i.e. with measured flux density increases of 20% – consistent with typical low-luminosity active galactic nuclei variability

Table 1. Summary of MAGIC GC observations by year.

Year	2012	2013	2014	2015
Obs. time [h]	3.0	25.9	27.2	11.2
Zd range [deg]	59–66	59–70	59–70	58–70

Notes. The listed observational times correspond to data surviving quality-selection cuts, as described in Sect. 2.3.

levels), the observational dataset accumulated by MAGIC still warrants a variability search in the VHE flux of the GC on a multi-year time scale.

In the following sections, we report on the results of this 4-yr observational campaign, covering the time period of the closest encounter between Sgr A* and G2.

2. The MAGIC observation campaign

2.1. The MAGIC Telescopes

The MAGIC (Major Atmospheric Gamma Imaging Cherenkov) telescopes are two 17 m diameter IACTs, located at an altitude of 2200 m a.s.l. at the Roque de los Muchachos Observatory on the Canary Island of La Palma, Spain (28°N, 18°W).

The telescopes are used to record flashes of Cherenkov light produced by Extensive Air Showers (EAS) initiated in the upper atmosphere by gamma-ray photons with energies $\gtrsim$50 GeV. Both telescopes are nominally operated together in a so-called stereoscopic mode, in which only events simultaneously triggering both telescopes are recorded and analyzed (Aleksić et al. 2016). For low zenith distance (Zd) observations and for $E > 220$ GeV, the integral sensitivity of MAGIC is $(0.66 \pm 0.03)\%$ in units of the Crab Nebula flux (C.U.) for 50 h of observations (Aleksić et al. 2016).

2.2. Observations

The GC region has been observed between April 2012 and July 2015, with 67 h of good-quality data collected. When observed from the MAGIC site, the GC culminates at a zenith distance of Zd = 58° and the time frame for observing the GC with MAGIC at Zd < 70° is from mid-February until the end of September. A breakdown of the observation time per year, along with the relevant Zd range is shown in Table 1.

Observing at such large zenith distances (58° to 70° Zd) increases the energy threshold (defined as the peak in the distribution of detected gamma-ray events binned in energy, estimated using Monte Carlo simulations) of MAGIC to a range between ~360 GeV and ~1.2 TeV (in general it varies with the zenith distance as $E_{\rm th,MAGIC} \sim \cos^{-2.3}$ (Zd), Aleksić et al. 2016), but at the same time it also increases the effective collection area for gamma rays by nearly one order of magnitude. Figure 1 shows the comparison of two collection areas (post analysis-cuts) versus energy obtained from Monte Carlo simulations; corresponding to the zenith distance distribution covered by the MAGIC GC observations, and to a typical low-Zd (5°−35°) observation.

The observations of the GC have been conducted in the False-Source tracking mode (also known as "Wobble" mode; Fomin et al. 1994), meaning that the telescopes were pointed to four different symmetric positions at a distance of 0.4° from
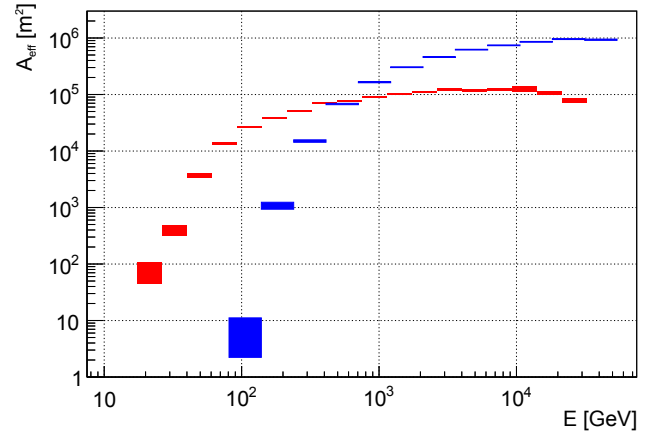
Fig. 1. Effective collection area computed from Monte Carlo simulated events matching the zenith and azimuth distribution of the presented GC observation and after all cuts that were applied for computing the energy spectrum and light-curve (blue). The collection area for a typical low zenith angle (5°−35°) observation is shown in red for comparison. One can clearly note the effect on the energy threshold and effective area due to the larger Zd.

Sgr A*. With this observation technique, the background can be estimated from regions with the same camera acceptance.

2.3. Data analysis

The data have been analyzed with the MAGIC standard analysis chain MARS (MAGIC Analysis and Reconstruction Software, Zanin et al. 2013). This chain includes the quality selection of the accumulated observations. During this step, the data are cleaned by removing events detected during periods of bad weather and/or during known temporary hardware issues. This basic data selection is performed based on several measured quantities, such as the mean photomultiplier currents, the event trigger rate, a measure of the amount of clouds in the field of view (based on measurements with an infra-red pyrometer and the LIDAR system, Gaug et al. 2014; Fruck et al. 2014) and the number of stars detected by the MAGIC star-guider cameras during the observations.

Due to the nature of the large-Zd observations of the GC (i.e. longer light path through the atmosphere), there is a larger impact on the quality of the recorded data due to a corresponding increase in the scattering of star light and decrease in the optical transmission of the atmosphere. To minimize these effects, strong quality cuts have been applied to the data. We have excluded periods of data taking when the photomultiplier currents were above twice the typical dark-night levels and also periods of data taking when the star-count reported by the star guider dropped below 70% of the median value. A cut on the data acquisition rate (dominated by the background cosmic-ray events) at ±30% of the typical value was applied as well, so that any data-taking periods when the event rates fluctuated substantially from the calculated mean rate were discarded.

The remaining events were cleaned to remove the contributions of the night sky background and electronic noise. After that, the resulting shower images were parametrized in terms of the so-called Hillas (Hillas 1985) and stereo parameters (*disp*, shower height). Based on the MC simulated gamma rays and real background events, recorded in a sky region free of gamma-ray sources, the Random Forest technique (Aleksić et al. 2012; Albert et al. 2008) was used for event classification in order to substantially reduce the contribution of hadronic air-showers.

Finally, an integration radius of 0.1° around the coordinates of Sgr A* (RA = 17:45:40, Dec = −29:00:28) was used for extraction of the gamma-ray excess, which was later used to produce the energy spectrum and the light-curve of the source[1]. An aperture of fixed size has been used in order to minimize the effect of an energy dependent point spread function (PSF) in the context of an extended component in the source. The aperture size value of 0.1° was also chosen to ensure that the results of this analysis can be more easily compared with previous measurements (e.g., Aharonian et al. 2009; H.E.S.S. Collaboration 2016). The background rate within the 0.1° integration radius has been calculated from a smoothed and modeled background estimation.

Shower images with size <50 ph.e. (photo-electrons) were discarded from the analysis in order to remove poorly reconstructed events. For the morphological study of the GC region, an *a-priori* cut on shower image size (200 ph.e. per telescope) was utilized to select only higher energy events ($E \gtrsim 1$ TeV). This ensures that only well reconstructed events contribute to the sky maps shown in Fig. 5, giving us a better signal-to-noise ratio and angular resolution.

The background in the skymap is mostly caused by diffuse hadronic and electron events, and is estimated using the so-called Blind Map technique. This technique compares event rates for each bin in camera coordinates for different Wobble pointing positions and calculates the background model as the median for each of the pixels. In this way, regions that are affected by an increased number of counts due to a source contribution are automatically avoided. The merit of this method is that it does not rely on an a-priori knowledge of the source location (and extension) in the field of view. The caveat of this methodology is that sources with an extension larger than the distance between the Wobble positions (0.4 deg in radius, for these observations) would start contributing to the background model. At the same time this technique is suitable for point sources or moderately extended sources, regardless of their position in the FoV.

We have estimated the systematic uncertainty of our measurements based on Aleksić et al. (2016); yielding less than a 15% systematic uncertainty on the energy scale, 11–18% for the flux normalization and ≲0.02 deg for the pointing accuracy. These numbers were determined at low and medium zenith distances and may therefore be underestimations for the data presented here due to the large average zenith distance of the observations. A separate paper concerning this topic is currently in preparation. In the spectral energy distribution (SED) plots we show the effect of the systematic uncertainties by drawing four gray crossed arrows for different energy regimes. The vertical arrow indicates the systematic uncertainty on the flux scale. The systematic bias on the energy scale also leads to an error in the calculation of the SED, which depends on the shape of the collection area energy dependence. The resulting effect is depicted with the inclined arrows representing the influence of the systematic uncertainty of the energy reconstruction.

3. Results

After applying the quality cuts described in Sect. 2.3, the remaining 67 h dataset yields a clear gamma-ray excess of events with $E > 1$ TeV at the location of Sgr A* with a significance of 27 standard deviations (using formula 17 of Li & Ma 1983).

---

[1] Using this aperture photometry method, part of the extended emission from the GC ridge (Aharonian et al. 2006b) may contribute at some degree to the measured flux.
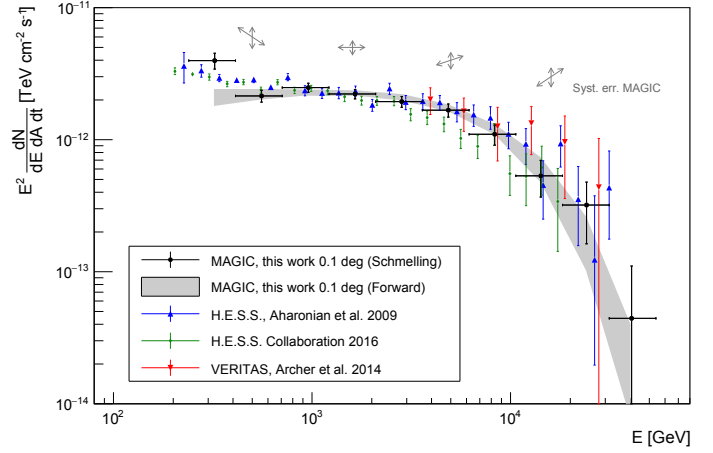
Fig. 2. SED of the Galactic center gamma-ray source measured by MAGIC between 2012 and 2015, unfolded with the method of Schmelling (1994; black data points), and the forward folding fit result, assuming a power-law with exponential cut-off (shaded area, see Sect. 3.1 for details). Previous measurements by H.E.S.S and VERITAS are also shown for comparison. The gray arrows indicate the estimated systematic uncertainty of our measurements for different energy ranges (see Sect. 2.3), considering also the slope of the effective collection area vs. energy.

3.1. Gamma-ray emission spectrum

The SED of Sgr A* in the energy range 300 GeV−40 TeV, unfolded with the method described in Schmelling (1994), is shown in Fig. 2. The spectral shape has been found to be well described by a power-law with an exponential cut-off,

$$\frac{\mathrm{d}F}{\mathrm{d}E} = f_0 \left(\frac{E}{E_0}\right)^{-\alpha} \exp\left(-\frac{E}{E_{\text{cut}}}\right). \tag{1}$$

The fit parameters of this model were obtained from the forward-folding fit to the measurements, which starts with the assumed spectrum and propagates it to detector counts using the response functions of the telescope. The latter included the MAGIC energy-migration matrix obtained from Monte Carlo simulations. This resulted in a fit with χ^2/N.D.F. = $9.1/11$ (*p*-value is 0.61, N.D.F. stands for the number of degrees of freedom), and the following parameters: $f_0 = (7.26 \pm 0.89) \times 10^{-13}$ cm^{-2} s^{-1} TeV^{-1}, $\alpha = 1.85 \pm 0.13$, $E_{\text{cut}} = (7.57 \pm 2.29)$ TeV. The fit is normalized at $E_0 = 2$ TeV.

The above uncertainties should be treated with caution when used separately, as the fit parameters are significantly correlated between each other. To estimate this correlation we used a Markov chain Monte Carlo (MCMC) approach (*emcee* algorithm: Goodman & Weare 2010; Foreman-Mackey et al. 2013) to sample the relevant parameter space and compute confidence contours. The sampling function used in the MCMC method was based on the Poissonian distribution, but was constructed to represent the likelihood of measuring a certain number of counts in the source region, given the model parameters and number of background events. The sampling also included the uncertainty on the MAGIC collection area, estimated from a dedicated Monte Carlo simulation which is part of the MAGIC standard analysis chain. The *emcee* algorithm samples the parameter space with a large number of "walkers", reproducing the posterior probability density function (PDF) for f_0, E_{cut} and α given the analyzed data sample. For simplicity in presentation, we have projected these distributions onto two-dimensional planes "$f_0 − \alpha$", "$f_0 − E_{\text{cut}}$" and "$\alpha − E_{\text{cut}}$", integrating over the third,
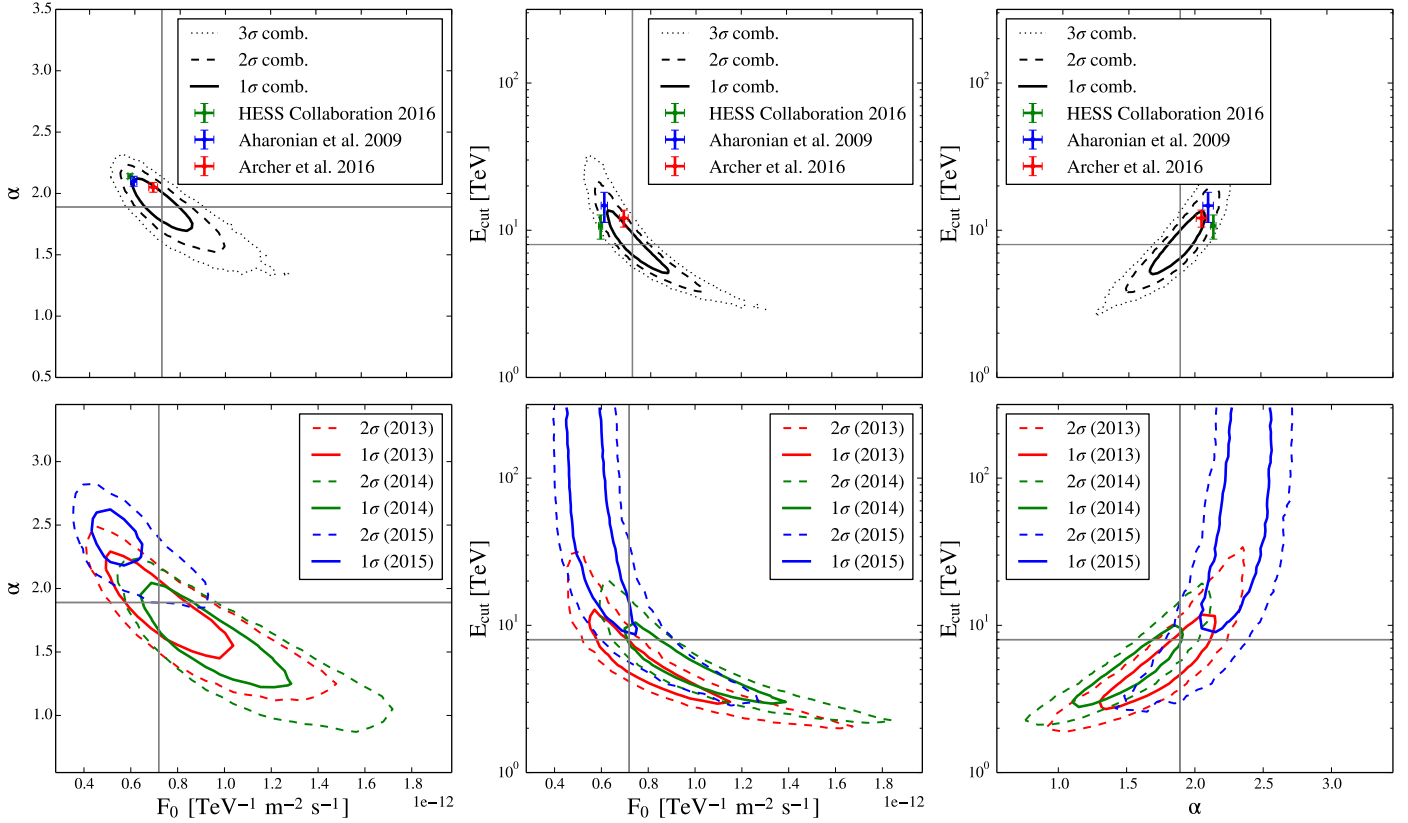
Fig. 3. *Top*: 2D projections of the probability distribution in the parameter space of the SED fit for the combined 2012–2015 dataset. The SED was fit using a power-law with exponential cut-off model (see Sect. 3.1). The gray cross-hair marks the best fit values found in this work. The red and blue data points mark the best fit values and uncertainties as measured by H.E.S.S. (Aharonian et al. 2009) and H.E.S.S. with VERITAS combined (Archer et al. 2016). *Bottom*: the same for the 2013 (red), 2014 (green) and 2015 (blue) seasons separately. The contours correspond to 1, 2 and 3 (only for the full dataset, *top*) σ confidence levels.

remaining parameter. The resulting containment contours, corresponding to 1, 2 and 3σ confidence levels, are shown in the top panel of Fig. 3.

The obtained results are compatible with previous measurements by the H.E.S.S. (Aharonian et al. 2009) and VERITAS (Archer et al. 2014) experiments at $\sim 1\sigma$ confidence level. At the same time we note that the updated H.E.S.S. spectrum of the source (H.E.S.S. Collaboration 2016) deviates from our measurements by $\gtrsim 2\sigma$.

3.2. Search for variability

We conducted a search for variability in the measured flux from Sgr A* during the period of observations. Note that the predicted closest approach of the G2 object was to happen in 2013/14. Figure 4 shows the light curves of the integral flux F for $E > 1$ TeV and $E > 10$ TeV, respectively. Detailed information about the individual measurements can be found in Tables 2 and 3. In both cases the light curves are consistent with a constant flux assumption. For $E > 1$ TeV, the fractional variability is less than 15%.

Additionally, we also searched for signatures of any spectral variability of the source during the periods of observation. To achieve this for the seasons 2013, 2014 and 2015 we separately fitted the spectrum of Sgr A* and compared the obtained parameters (the 2012 season was not fit due to the limited dataset). We used the MCMC approach described above to sample the parameter space for each season separately. The

parameter cross-correlation diagrams for three years of MAGIC observations are shown in the lower panel of Fig. 3. They do not show any significant variation between the different observational seasons.

3.3. Morphology of the emission

The region within one degree around the GC contains a collection of known gamma-ray sources. Apart from the point-like source component at the coordinates of Sgr A*, MAGIC also detects emission from the known composite supernova remnant G0.9+0.1 (Aharonian et al. 2005), at the level of 9σ local significance. A sky map of the GC region as seen by MAGIC is provided in Fig. 5 (left), which shows the relative count number (with respect to the remaining background) of the gamma-ray events with $E \gtrsim 1$ TeV. The extended emission becomes more obvious if the gamma-ray flux contributions from Sgr A* and G0.9+0.1 are removed from the image. For this we subtract a sum of two symmetric 2D Gaussians – the PSF model, which provides a reasonable description of the MAGIC PSF (Aleksić et al. 2016), from the fitted coordinates of Sgr A* and G0.9+0.1. The shape parameters (kernel of the first 2D Gaussian $\sigma_1 = 0.048 \pm 0.007\,^\circ$, kernel of the second 2D Gaussian $\sigma_2 = 0.092 \pm 0.015\,^\circ$, normalization ratio in terms of the second component $N_2/N_{tot} = 0.51 \pm 0.18$) of the PSF model have been determined with a χ^2 fit to Crab Nebula data recorded at a similar Zd. The result of the subtraction is shown in the right panel of Fig. 5. The residual sky map shows the extended
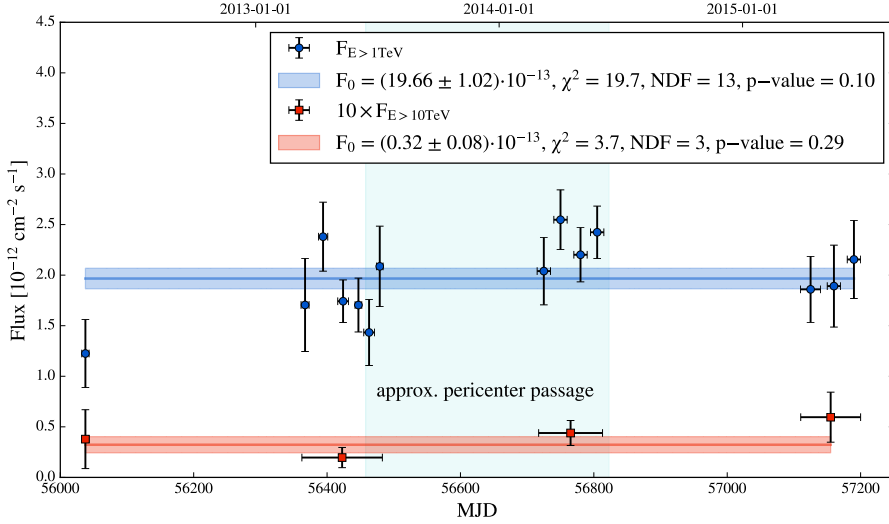
Fig. 4. Light curves of the integral gamma-ray flux from the Galactic center for $E > 1$ TeV and $E > 10$ TeV. The red and blue lines represent the best fits to the constant flux, the corresponding shaded regions represent the 1σ confidence intervals. For $E > 1$ TeV the bins span over 10–30 days, whereas the yearly binning has been chosen for $E > 10$ TeV because of the low event count rate. The flux values of the latter have been multiplied by 10 for better visibility in the plot. Detailed information for each data point is given in Tables 2 and 3.

Table 2. Summary of the MAGIC flux measurements used in the light curve for $E > 1$ TeV.

Range [MJD–50 000]	6032–6043	6362–6373	6387–6401	6416–6432	6442–6452	6455–6471	6474–6483
Observational time [h]	3.0	1.5	3.5	8.5	6.5	3.7	2.2
Detection significance [σ]	4.9	4.1	7.5	9.2	6.6	5.2	5.6
Flux [10^{-12} s^{-1} cm^{-2}]	1.23 ± 0.34	1.71 ± 0.46	2.38 ± 0.34	1.74 ± 0.27	1.70 ± 0.27	1.43 ± 0.33	2.09 ± 0.40
Range [MJD–50 000]	6717–6735	6740–6760	6770–6790	6795–6813	7110–7140	7150–7170	7180–7200
Observational time [h]	5.9	5.8	7.8	7.7	4.5	2.3	3.1
Detection significance [σ]	5.9	9.3	8.8	10.1	6.1	5.4	6.4
Flux [10^{-12} s^{-1} cm^{-2}]	2.04 ± 0.33	2.55 ± 0.30	2.20 ± 0.27	2.42 ± 0.26	1.86 ± 0.33	1.89 ± 0.45	2.15 ± 0.39

**Table 3.** Summary of the MAGIC flux measurements used in the light curve for $E > 10$ TeV.

Range [MJD–50 000]	6032–6043	6363–6482	6719–6812	7110–7200
Observational time [h]	3.0	25.9	27.2	11.2
Detection significance [σ]	1.0	1.8	4.3	2.7
Flux [10^{-14} s^{-1} cm^{-2}]	3.5 ± 3.4	3.0 ± 1.3	5.2 ± 1.5	7.9 ± 3.0

emission from the region along the Galactic plane, similar in shape with the earlier findings (shown as dashed green contours Aharonian et al. 2006b), though detected here at higher energies.

In addition, a source of significant VHE gamma-ray emission located close to the GCA (Tsuboi et al. 1997), 0.2° to the east of Sgr A*, has been detected at a 7.2σ local (6.4σ post-trials) significance level. The significance was evaluated through a test statistic based on the background emission that corresponds to the position of the source in terms of camera coordinates but is measured in the Off-source region. The VHE excess is consistent with a point-source at the coordinates RA 17:46:25, Dec −28:52:55 with an error circle of 0.03 deg, determined by fitting a single 2D Gaussian shape. Throughout this paper we refer to this source as MAGIC J1746.4-2853. We note that it is positionally consistent with the VHE excess VER J1746-289, recently reported by Archer et al. (2016), and previously presented by the MAGIC (Fruck et al. 2015), H.E.S.S. (Lemiere et al. 2015) and VERITAS (Smith 2015) collaborations. Also the EGRET source 3EG J1746-2851 and the *Fermi* source 3FGL J1746.3-2851c are in spatial coincidence with the VHE source.

The inset in the right panel of Fig. 5 shows the best fit coordinates of MAGIC J1746.4-2853, VER J1746-289, and HESS J1746-285, with error bars containing the 68% C.L. (90% in case of HESS J1746-285) statistical-fit uncertainty only. The errors for the other two sources have been taken from Archer et al. (2016) and Lemiere et al. (2015) but rotated from the Galactic to Equatorial coordinate frame. The systematic pointing error of MAGIC is estimated to be ≲0.02 deg, while Archer et al. (2016) state a systematic pointing error of 0.013 deg in both Galactic latitude and longitude.

The origin of this new source is unclear, though several possible associations with known objects can be speculated upon. One possible candidate is the giant molecular cloud (GMC) G0.11-0.11, located very close to the southern half of the GCA, and between the GCA and Sgr A*. Gamma-ray emission could either originate from electrons accelerated in the interaction of G0.11-0.11 with the GCA (such a scenario was already discussed by Pohl 1997), or from CR interactions inside the dense molecular material in the region. Those cosmic rays could either originate from past active episodes of Sgr A*, several hundreds or thousands of years ago, or they could have been accelerated in shocks associated with the numerous supernova explosions that
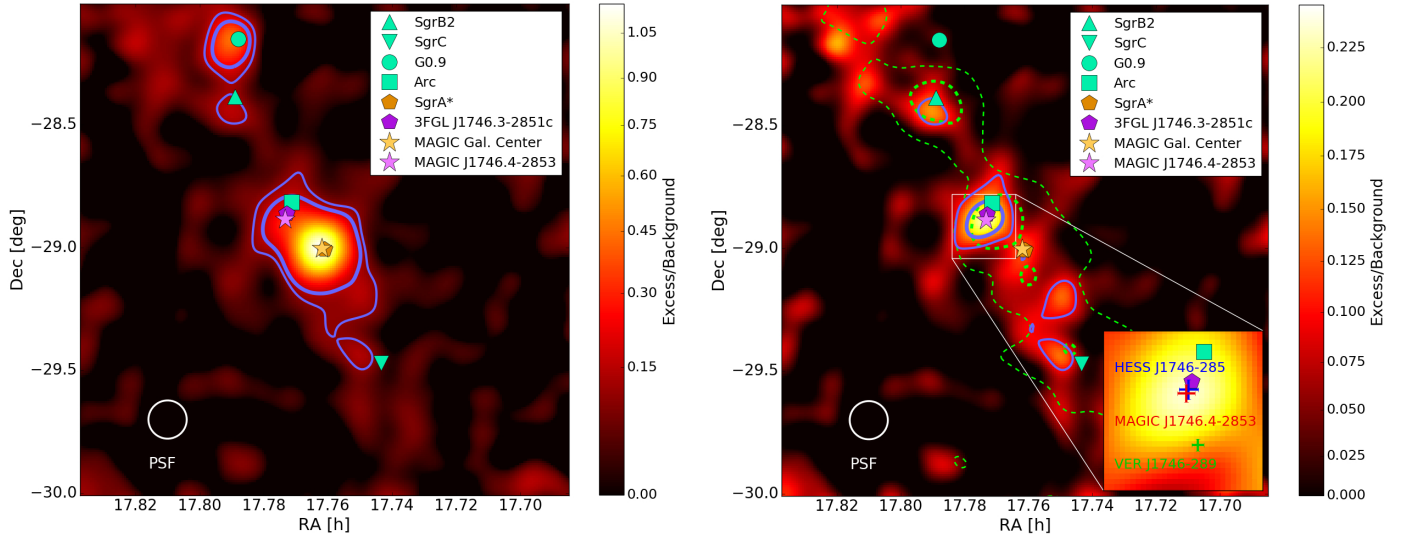
Fig. 5. *Left*: a sky map of the central 2 deg × 2 deg field of view around the Galactic center position, showing the relative signal to background count rate for $E \gtrsim 1$ TeV. *Right*: the same, with the Sgr A* and G0.9+0.1 point sources subtracted from the map (see the details in the text). Both sky maps have been smeared with a Gaussian kernel ($\sigma_{ker} = 0.055°$) and are given in units of relative counts (number of excess events over the number of estimated background events using the Blind Map method). The blue contours show 3σ (thin) and 5σ (thick) local significance levels. Coordinates of the known radio structures are indicated with light green markers. The best-fit coordinates of the Galactic center source and of the unidentified source (here referred to as MAGIC J1746.4-2853) are indicated with stars. The coordinates of Sgr A* (radio) and the *Fermi* source 3FGL J1746.3-2851c are indicated by pentagons. The MAGIC PSF is given as a 1σ contour of a 2D Gaussian smeared with the same kernel that was used for the sky map. For comparison, the H.E.S.S. contours at the event count levels of 320 and 360 are shown as dashed lines (Aharonian et al. 2006b). Please note that the H.E.S.S contours correspond to the energy threshold of 380 GeV – significantly different from that of MAGIC (~1 TeV) for these skymaps. The inset in the lower right shows a zoom-in onto the Arc region with best fit coordinates of MAGIC J1746.4-2853, VER J1746-289, and HESS J1746-285 shown as error crosses (Archer et al. 2016; Lemiere et al. 2015), describing statistical errors from the fit only[2].

have been driving the expansion of the GMC (Oka et al. 2001). The analysis of the X-ray data suggests, alternatively, a possible association with a pulsar wind nebula candidate found within the positional uncertainty of the source (Lemiere et al. 2015).

4. Discussion

The primary motivation behind this observing campaign was to search for any flaring emission that may occur due to the passage of the G2 object near to the SMBH at the center of the Milky Way galaxy. The proximity of the passage of the G2 object to the SMBH could have provided a unique opportunity to study the process of accretion of an Earth-mass body onto a black hole, as well as addressing several questions regarding particle-acceleration mechanisms near to a SMBH. However, the results of recent observations at other wavelengths suggest that the G2 object has not been disrupted by its proximity to the SMBH, therefore it is perhaps not surprising that no evidence for an enhancement in the VHE flux of Sgr A* was found.

Regardless, 10 yr after the discovery of VHE emission from the region, the nature of the γ-ray source at the GC remains uncertain. The MAGIC observational campaign also aimed to help clarify this issue, by measuring both the overall spectral shape and variability of Sgr A* in the energy range above several hundreds of GeV.

The theoretical expectations for the spectral shape and flux variability significantly vary between the different assumed

scenarios. Before the publication of the *Fermi* spectrum on Sgr A* (Chernyakova et al. 2011), the models were built mainly around the TeV emission observed by H.E.S.S. (Aharonian et al. 2004, 2009). The MAGIC observations presented here confirm the previous measurement of the source SED and extend it up to ~50 TeV, providing a new test for both hadronic and leptonic type scenarios, proposed for explaining the observed VHE emission from Sgr A*, as shown in Fig. 6.

In most of the hadronic scenarios, the gamma rays are produced by π^0 decay from the interactions of cosmic rays (CRs), accelerated in the vicinity of the SMBH, with the dense environment close to the GC. In the model of Ballantyne et al. (2011), the measured TeV spectrum is obtained by switching on and off CR acceleration close to the SMBH at specific times in the past. The energy dependence of the diffusion coefficient is then responsible for the spectral shape. One implication of the Ballantyne et al. (2011) model is that variability of the TeV spectrum ($\gtrsim 10$ TeV) is expected on time scales of the order of 10 yr, not only in the case that the accelerator stays quiet, but also if a new episode of CR acceleration occurs. According to the MAGIC results, there is no strong evidence for variable emission from Sgr A* at these energies over the years 2012–2015, as well as with respect to previous measurements.

After discovery of a point-source in the *Fermi* data (1FGL J1745.6-2900), which could be associated with the H.E.S.S. TeV source (HESS J1745-290), Chernyakova et al. (2011) and later Linden et al. (2012) proposed similar hadronic models, able to explain both the GeV and the TeV emission. These models use the injection spectrum resulting from CR acceleration close to the SMBH with a spectral index $\alpha \sim 2$ and an exponential cut-off at ~100 TeV. The variation of the spectral index of the gamma-ray emission along the spectrum is explained

---

[2] The statistical pointing errors of the best fit coordinates for VER J1746-289 and HESS J1746-285 in Fig. 5 have been obtained by transformation of the values, which are given in Galactic coordinates, into the Equatorial system by coordinate rotation. The errors on the position of HESS J1746-285 correspond to 90% C.L.
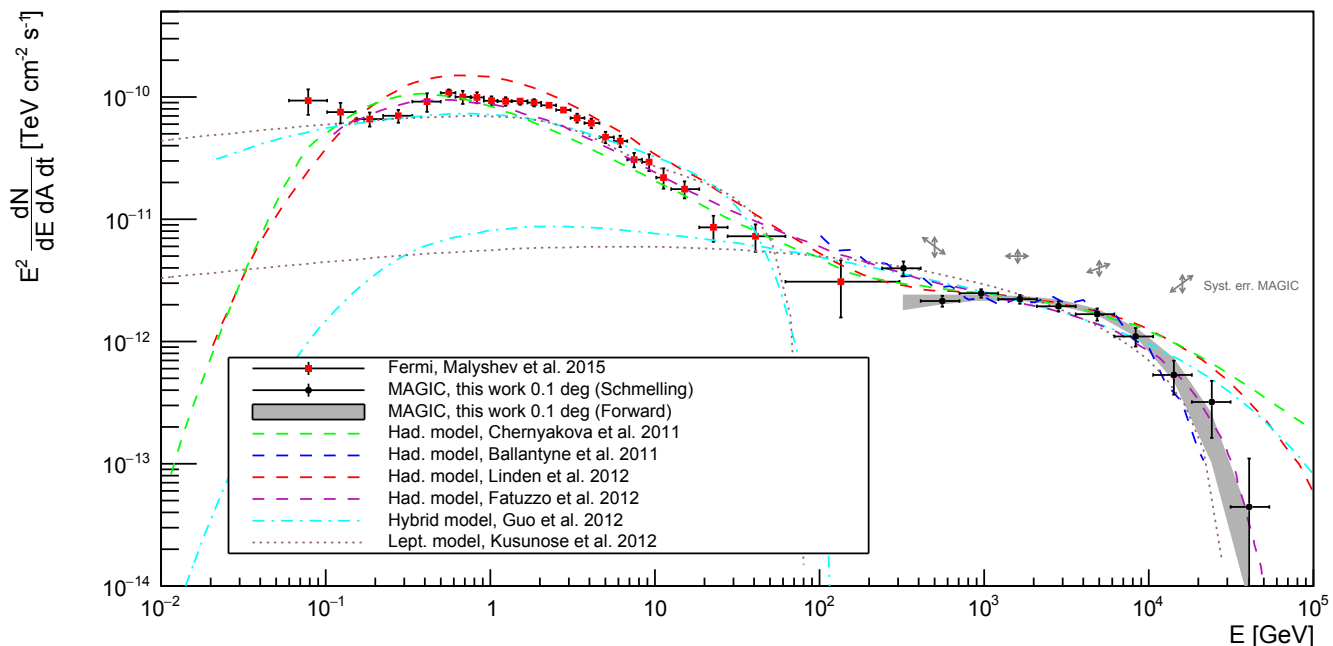
Fig. 6. GeV–TeV SED of SgrA*. The *Fermi* data points in the ~100 MeV−100 GeV band are from the most recent spectrum of Malyshev et al. (2015). Contemporary hadronic (dashed), leptonic (dotted) and hybrid-type (dash-dotted) models are shown for comparison.

by the difference in the diffusion times for GeV and TeV cosmic rays. Both models are assuming a dense configuration of interstellar gas at distances from one to a few parsecs away from Sgr A*.

In their hadronic model, Fatuzzo & Melia (2012) include a simplified description of the particle acceleration in their numeric simulation of the diffusion of CRs through the turbulent magnetic fields expected around Sgr A*. They assume a torus of dense material around the GC SMBH of about 2 pc in radius, embedded inside a wind zone of lower density, about 10 pc in diameter. Particles are accelerated throughout their diffusion history and eventually react with the ambient protons, either in the torus (generating HE emission) or in the wind zone (generating VHE emission). This model does not need time variability to explain the overall shape of the GeV–TeV spectrum.

Alternatively, Kusunose & Takahara (2012) suggested a model where high-energy electrons are accelerated close to the central SMBH and interact via inverse-Compton scattering with soft photons, emitted by the dense population of stars and dust inside the central few parsecs of the GC. The electron populations would have to originate from different acceleration mechanisms or sources. A similar scenario is also suggested by Hinton & Aharonian (2007).

A hybrid lepto-hadronic scenario was also recently suggested by Guo et al. (2013). In their model both electrons and protons are accelerated in the vicinity of the SMBH. The GeV part of the spectrum is attributed to the inverse-Compton scattering of relativistic electrons on the soft background photons, while the TeV emission is produced via the CRs colliding with the surrounding gas.

Hadronic scenarios have recently gained support through the measurement of gamma rays with energies up to over 40 TeV, which the authors (H.E.S.S. Collaboration 2016) interpreted as evidence for the presence of PeV protons in the region. Despite the temptation to link their presence to Sgr A*, this is not straightforward due to the required energetics, exceeding the current bolometric luminosity of the source and the availability of

alternative scenarios (H.E.S.S. Collaboration 2016). Regardless, such a connection is still considered very likely.

Considering the statistical and systematic errors on the Sgr A* spectrum as measured by MAGIC, no single emission model can be unequivocally ruled out. See Fig. 6 for an overview of contemporary modeling attempts presented alongside MAGIC and recent *Fermi* data. The SED is in a reasonable agreement with the leptonic and hybrid type models, shown with the dotted (Kusunose & Takahara 2012) and dash-dotted (Guo et al. 2013) lines. Hadronic models seem to conflict with the lowest energy (60–100 MeV) *Fermi* measurements (Malyshev et al. 2015). However, to be able to distinguish between the various models, the study of flux variations over time, as predicted by most of the hadronic models, will have the highest separation power. So far the *Fermi* observations in the GeV band have not yet revealed any significant variability (Chernyakova et al. 2011) and the MAGIC monitoring in the TeV band presented here, also measures a stable source flux. However it is still necessary to continue monitoring Sgr A*, especially at the highest energies, where the most rapid variability on a timescale of the order of 10 yr is predicted (Ballantyne et al. 2011). For now, the absence of any detection of variability prevents the use of these measurements to disentangle the various emission models from each other.

5. Conclusions

The GC region has been observed with the MAGIC telescopes between 2012 and 2015, collecting 67 h of good-quality data. No effect of the G2 object on the VHE gamma-ray emission from the GC was detected during the 4 yr observation campaign. The lack of variability from the direction of Sgr A*, as measured by MAGIC, makes it difficult to rule out single models describing particle acceleration and gamma-ray emission mechanisms at the source. These observations may still prove useful as an accurate measurement of the baseline emission from Sgr A* in the case of any possible flaring activity in the future.

Along with the variability study, the large exposure of 67 h allowed us to derive a precise energy spectrum of Sgr A*, which agrees with previous measurements within errors. Furthermore we were able to study the morphology of the GC region. As a result of this study, we confirm the detection in the VHE gamma-ray band of the supernova remnant G0.9+0.1, and report the detection with MAGIC of a VHE source of unknown nature in the region of the GC radio arc.

References

Acero, F., Aharonian, F., Akhperjanian, A., et al. 2010, MNRAS, 402, 1877
Aharonian, F., & Neronov, A. 2005, ArXiv e-prints [arXiv:astro-ph/0503354]
Aharonian, F., Akhperjanian, A., Aye, K.-M., et al. 2004, A&A., 425, L13
Aharonian, F., Akhperjanian, A., Aye, K.-M., et al. 2005, A&A, 432, L25
Aharonian, F., Akhperjanian, A., Bazer-Bachi, A., et al. 2006a, ApJ, 636, 777
Aharonian, F., Akhperjanian, A. G., Bazer-Bachi, A. R., et al. 2006b, Nature, 439, 695
Aharonian, F., Akhperjanian, A., Anton, G., et al. 2009, A&A, 503, 817
Albert, J., Aliu, E., Anderhub, H., et al. 2006, ApJ, 638, L101
Albert, J., Aliu, E., Anderhub, H., et al. 2008, Nucl. Instrum. Meth. Phys. Res. A, 588, 424
Albert, J., Aliu, E., Anderhub, H., et al. 2007, Nucl. Instrum. Meth. Phys. Res. Section A: Accelerators, Spectrometers, Detectors and Associated Equipment, 583, 494
Aleksić, J., Alvarez, E. A., Antonelli, L. A., et al. 2012, Astropart. Phys., 35, 435
Aleksić, J., Ansoldi, S., Antonelli, L. A., et al. 2016, Astropart. Phys., 72, 76
Archer, A., Barnacka, A., Beilicke, M., et al. 2014, ApJ, 790, 149
Archer, A., Benbow, W., Bird, R., et al. 2016, ApJ, 821, 129
Atoyan, A., & Dermer, C. D. 2004, ApJ, 617, L123
Baganoff, F., Bautz, M., Cui, W., et al. 2000, in BAAS, 32, 1184
Baganoff, F. K., Bautz, M. W., Brandt, W. N., et al. 2001, Nature, 413, 45
Baganoff, F. K., Maeda, Y., Morris, M., et al. 2003, ApJ, 591, 891
Ballantyne, D. R., Schumann, M., & Ford, B. 2011, MNRAS, 410, 1521
Bartos, I., Haiman, Z., Kocsis, B., & Márka, S. 2013, Phys. Rev. Lett., 110, 221102
Bertero, M. 1989, in Advances in Electronics and Electron Physics, vol. 75, ed. P. W. Hawkes, 1
Bower, G. C., Markoff, S., Brunthaler, A., et al. 2014, ApJ, 790, 1
Bower, G. C., Markoff, S., Dexter, J., et al. 2015, ApJ, 802, 69
Chernyakova, M., Malyshev, D., Aharonian, F. A., Crocker, R. M., & Jones, D. I. 2011, ApJ, 726, 60
Enomoto, R., Mori, M., & Yanagita, S. 2003, The Universe Viewed in Gamma-rays, Frontiers Science Series (Universal Academy Press)
Fatuzzo, M., & Melia, F. 2012, ApJ, 757, L16
Fish, V. L., Doeleman, S. S., Beaudoin, C., et al. 2011, ApJ, 727, L36
Fomin, V. P., Stepanian, A. A., Lamb, R. C., et al. 1994, Astropart. Phys., 2, 137
Foreman-Mackey, D., Hogg, D. W., Lang, D., & Goodman, J. 2013, PASP, 125, 306
Fruck, C., Gaug, M., Zanin, R., et al. 2014, ArXiv e-prints [arXiv:1403.3591]
Fruck, C., Ward, J., Vovk, I., et al. 2015, in PoS(ICRC2015)859
Gaug, M., Blanch, O., Dorner, D., et al. 2014, ArXiv e-prints [arXiv:1403.5083]
Genzel, R., Eisenhauer, F., & Gillessen, S. 2010, Rev. Mod. Phys., 82, 3121

Genzel, R., Schödel, R., Ott, T., et al. 2003, Nature, 425, 934
Ghez, A. M., Witzel, G., Sitarski, B., et al. 2014, ATel, 6110, 1
Giannios, D., & Sironi, L. 2013, MNRAS, 433, L25
Gillessen, S., Genzel, R., Fritz, T., et al. 2012, Nature, 481, 51
Gillessen, S., Genzel, R., Fritz, T. K., et al. 2013a, ApJ, 763, 78
Gillessen, S., Genzel, R., Fritz, T. K., et al. 2013b, ApJ, 774, 44
Goodman, J., & Weare, J. 2010, Commun. Appl. Math. Comput. Sci., 5, 65
Guo, Y.-Q., Yuan, Q., Liu, C., & Li, A.-F. 2013, J. Phys. G Nucl. Phys., 40, 065201
H.E.S.S. Collaboration 2016, Nature, 531, 476
Hillas, A. M. 1985, Int. Cosmic Ray Conf., 3, 445
Hinton, J. A., & Aharonian, F. A. 2007, ApJ, 657, 302
Kistler, M. D. 2015, ArXiv e-prints [arXiv:1511.01159]
Kosack, K., Badran, H., Bond, I., et al. 2004, ApJ, 608, L97
Kusunose, M., & Takahara, F. 2012, ApJ, 748, 34
Lemiere, A., Terrier, R., Jouvin, L., et al. 2015, in PoS(ICRC2015)838
Li, T.-P., & Ma, Y.-Q. 1983, ApJ, 272, 317
Linden, T., Lovegrove, E., & Profumo, S. 2012, ApJ, 753, 41
Malyshev, D., Chernyakova, M., Neronov, A., & Walter, R. 2015, A&A, 582, A11
Mayer-Hasselwander, H. A., Bertsch, D. L., Dingus, B. L., et al. 1998, A&A, 335, 161
Meyer, L., Ghez, A. M., Do, T., et al. 2014, in AAS Meet. Abst., 223, 108.07
Mori, K., Hailey, C. J., Krivonos, R., et al. 2015, ApJ, 814, 94
Oka, T., Hasegawa, T., Sato, F., Tsuboi, M., & Miyazaki, A. 2001, PASJ, 53, 779
Pohl, M. 1997, A&A, 317, 441
Ponti, G., De Marco, B., Morris, M. R., et al. 2015, MNRAS, 454, 1525
Porter, T. A., Murgia, S., & the Fermi LAT Collaboration 2015, ArXiv e-prints [arXiv:1507.04688]
Schartmann, M., Burkert, A., Alig, C., et al. 2012, ApJ, 755, 155
Schmelling, M. 1994, Nucl. Instrum. Meth. Phys. Res. Section A: Accelerators, Spectrometers, Detectors and Associated Equipment, 340, 400
Shapiro, S. L., & Teukolsky, S. A. 1983, Black holes, white dwarfs, and neutron stars: The physics of compact objects (Wiley-VCH)
Smith, A. W. 2015, in PoS ICRC2015, 787
Tikhonov, A., & Arsenin, V. 1977, Solutions of ill-posed problems, Scripta series in mathematics (Winston)
Tsuboi, M., Ukita, N., & Handa, T. 1997, ApJ, 481, 263
van Eldik, C. 2015, Astropart. Phys., 71, 45
Wang, Q. D., Lu, F. J., & Gotthelf, E. V. 2006, MNRAS, 367, 937
Wang, Y.-P., Lu, Y., & Chen, L. 2009, Res. Astron. Astrophys., 9, 761
Weisskopf, M. C., Tananbaum, H. D., Van Speybroeck, L. P., & O'Dell, S. L. 2000, in Astronomical Telescopes and Instrumentation, International Society for Optics and Photonics, Proc. SPIE, 4012, 2
Witzel, G., Ghez, A. M., Morris, M. R., et al. 2014, ApJ, 796, L8
Yusef-Zadeh, F., Bushouse, H., Schödel, R., et al. 2015, ApJ, 809, 10
Zajacek, M., Eckart, A., Peissker, F., Karssen, G. D., & Karas, V. 2015, Proc. 24th Annual Conference of Doctoral Students – WDS 2015 – Physics, eds. J. Safrankova & J. Pavlu, Prague, Matfyzpress, 27
Zanin, R., Carmona, E., Sitarek, J., Colin, P., & Frantzen, K. 2013, in Proc. of the 33st International Cosmic Ray Conference, Rio de Janeiro, Brasil

[1] ETH Zurich, 8093 Zurich, Switzerland
[2] Università di Udine, and INFN Trieste, 33100 Udine, Italy
[3] INAF National Institute for Astrophysics, 00136 Rome, Italy
[4] Università di Siena, and INFN Pisa, 53100 Siena, Italy
[5] Università di Padova and INFN, 35131 Padova, Italy
[6] Croatian MAGIC Consortium, Rudjer Boskovic Institute, University of Rijeka, University of Split and University of Zagreb, 51000 Rijeka, Croatia
[7] Saha Institute of Nuclear Physics, 1/AF Bidhannagar, Salt Lake, Sector-1, 700064 Kolkata, India
[8] Max-Planck-Institut für Physik, 80805 München, Germany
[9] Universidad Complutense, 28040 Madrid, Spain
[10] Inst. de Astrofísica de Canarias, 38200 La Laguna, Tenerife, Spain
[11] University of Łódź, 90236 Lodz, Poland
[12] Deutsches Elektronen-Synchrotron (DESY), 15738 Zeuthen, Germany
[13] Institut de Fisica d'Altes Energies (IFAE), The Barcelona Institute of Science and Technology, Campus UAB, 08193 Bellaterra (Barcelona), Spain
[14] Universität Würzburg, 97074 Würzburg, Germany
[15] Institute for Space Sciences (CSIC/IEEC), 08193 Barcelona, Spain

[16] Technische Universität Dortmund, 44221 Dortmund, Germany

[17] Finnish MAGIC Consortium, Tuorla Observatory, University of Turku and Astronomy Division, University of Oulu, 90014 Oulu, Finland

[18] Unitat de Física de les Radiacions, Departament de Física, and CERES-IEEC, Universitat Autònoma de Barcelona, 08193 Bellaterra, Spain

[19] Universitat de Barcelona, ICC, IEEC-UB, 08028 Barcelona, Spain

[20] Japanese MAGIC Consortium, ICRR, The University of Tokyo, Department of Physics and Hakubi Center, Kyoto University; Tokai University, The University of Tokushima, KEK, Japan

[21] Inst. for Nucl. Research and Nucl. Energy, 1784 Sofia, Bulgaria

[22] Università di Pisa, and INFN Pisa, 56126 Pisa, Italy

[23] ICREA and Institute for Space Sciences (CSIC/IEEC), 08193 Barcelona, Spain

[24] Now at Centro Brasileiro de Pesquisas Físicas (CBPF/MCTI), R. Dr. Xavier Sigaud, 150 – Urca, 22290-180 Rio de Janeiro – RJ, Brazil

[25] Now at NASA Goddard Space Flight Center, Greenbelt, MD 20771, USA

[26] Humboldt University of Berlin, Institut für Physik Newtonstr. 15, 12489 Berlin Germany

[27] Also at University of Trieste, Italy

[28] Now at École polytechnique fédérale de Lausanne (EPFL), 1015 Lausanne, Switzerland

[29] Now at Max-Planck-Institut fur Kernphysik, PO Box 103980, 69029 Heidelberg, Germany

[30] Also at Japanese MAGIC Consortium, Kyoto, Japan

[31] Now at Finnish Centre for Astronomy with ESO (FINCA), 20014 Turku, Finland

[32] Also at INAF-Trieste and Dept. of Physics & Astronomy, University of Bologna, Italy

[33] Also at ISDC – Science Data Center for Astrophysics, 1290 Versoix (Geneva), Switzerland

[34] Universidad de La Laguna, Dpto. Astrofísica, 38206 La Laguna, Tenerife, Spain

[35] Now at Department of Physics and Department of Astronomy, University of Maryland, College Park, MD 20742, USA

Appendix A: Energy migration and unfolding of the MAGIC spectrum

The reconstruction of the energy of the primary gamma ray that initiated an air-shower has limited accuracy. The finite energy resolution results in migration of events between the neighboring energy bins, which may lead to significant spillovers from more to less populated energy bins. The measured event energy distribution for the MAGIC GC dataset – subject to this issue – is shown in Fig. A.1 with black points.

The standard MAGIC data analysis chain allows us to compensate for this via the inclusion of the energy migration effects in the spectrum reconstruction procedure. The amount of migration from each energy bin is determined from Monte Carlo simulations, updated for each MAGIC observational period. It is expressed in the form of the energy migration matrix, relating the original ("true") energy of the gamma-ray photon to that reconstructed by the analysis ("estimated" energy).

This migration matrix is then used to deconvolve (or unfold) the measured event distribution and reconstruct the original spectrum of an astrophysical source. The analysis procedure allows the indicative spectral shape to be supplied, which is then used to regularise the obtained solution. The detailed procedure is described in Albert et al. (2007). The MAGIC standard analysis requires several different unfolding techniques to be applied, with the result considered reliable only if all of them agree within the estimated uncertainties. These include the forward folding approach (the assumed spectral model is propagated through the MAGIC responses and its parameters are fit against the data) and three regularisation methods, further referred to as "Bertero" (Bertero 1989), "Schmelling" (Schmelling 1994) and "Tikhonov" (Tikhonov & Arsenin 1977).

The outcome of the application of these methods is shown in Fig. A.1, which summarises the measured (in terms of the estimated energy) and reconstructed (in terms of the true energy) event distributions. The true energy bins are wider than the measured energy bins, as required by the method, and show the magnitude of the spillover between energy bins.

We further used these event distributions to estimate the spectrum of the GC, corrected for the energy migration effects. The results from the unfolding techniques described above are shown in Fig. A.2. All the methods yielded results that are compatible, which indicates that the determination of the true spectrum from the measured one was done reliably. For the SEDs in the main part of this manuscript (in Figs. 2 and 6) we show the spectral data points obtained with the "Schmelling" technique, while, as it is commonly done in the MAGIC data analysis, the reported spectral fit results were obtained with the forward folding technique.

It is important to stress here, that the Sgr A* observations were taken over a range of zenith distances (see Table 1 in the
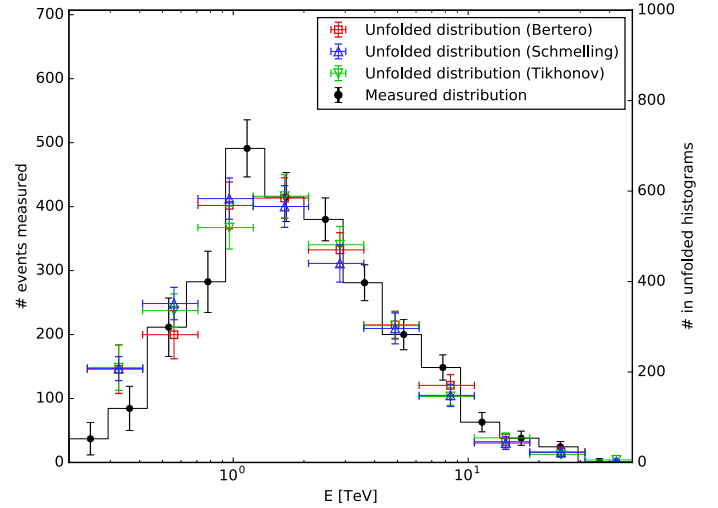
Fig. A.1. Energy distribution of the excess events in the SgrA* data sample. The measured event distribution in terms of estimated energy is shown in black and is accompanied with the corresponding unfolded distributions, displayed in "true" energy. The details of the procedure are given in Appendix A.
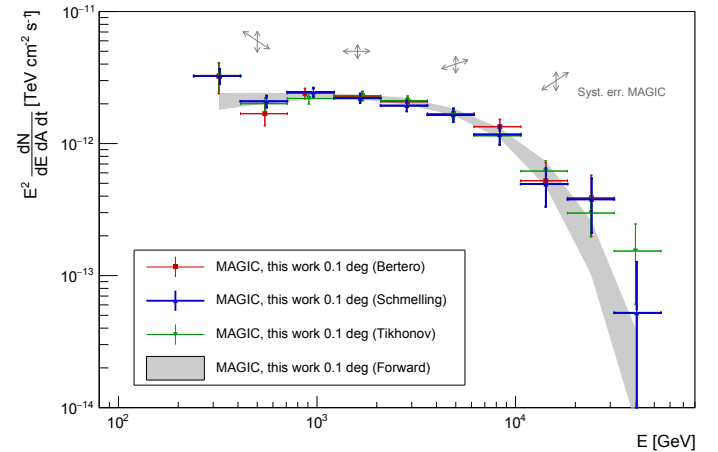
Fig. A.2. Unfolded SEDs of SgrA*, obtained with three different deconvolution techniques (see Appendix A and Fig. A.1). The gray arrows indicate the estimated systematic uncertainty (see also Sect. 2.3).

manuscript), where the energy threshold is changing fast, as illustrated in Sect. 2.2. This results in a broad distribution of the detected events versus the energy, as shown in Fig. A.1. The lowest-energy data points in SEDs in Figs. 2 and A.2 are dominated by the lowest zenith angles in our Sgr A* observations (<60 deg), which have the largest effective area at these energies (i.e., lowest energy threshold).